Inhibition of S-adenosylhomocysteine hydrolase (SAHH) Induces Fas Ligand Gene Expression and Apoptotic Death in Leukemic T Lymphocytes.

Harold Ghooray[1], Smita Ghare[1], Madhuvanti Patil[1], Swati Joshi-Barve[1,2], Craig J McClain[1,2], and Shirish Barve[1,2].
Department of Pharmacology and Toxicology[1] and Department of Medicine[2], University of Louisville Health Sciences Center, Louisville, KY 40202.

ABSTRACT

The transmethylation (TM) pathway is up regulated in activated proliferating T cells and transformed T leukemic cells but not in resting T cells, making it an ideal target to eliminate leukemic T cells. The TM pathway involves the methyltransferase-mediated donation of methyl groups by S-adenosylmethionine (SAM) and conversion of SAM to S-adenosylhomocysteine (SAH). SAH is a potent feedback inhibitor of methyltransferases and has the potential to influence DNA and histone methyltransferases affecting chromatin remodeling events that dictate gene expression. Under physiologic conditions SAH is hydrolyzed to adenosine and homocysteine by S-adenosylhomocysteine hydrolase (SAHH) which catalyzes the only reversible reaction in the TM pathway.

Conclusions: The present work was carried out to examine the effect of inhibiting SAHH on the survival of T leukemic cells. SAHH was inhibited in T cell leukemic cell lines – Jurkats and Molt-4 by using two distinct pharmacological agents - 3-deaza-adenosine (DZA) and 3-Deazaneplanocin A (DZneP). The data obtained showed that SAHH inhibition markedly decreases the cellular methylation potential and induces apoptotic death in T leukemic cells. Analysis of the molecular mechanisms underlying the apoptotic death demonstrated that SAHH inhibition leads the induction of FasL gene expression. We are currently examining the chromatin changes in the promoter region of the FasL gene that are induced by SAHH inhibition in T leukemic cells. Overall, the data indicate that SAHH could be a potential therapeutic target in the treatment of T leukemic cells.

INTRODUCTION

- T- cell leukemia is a rare and aggressive tumor that does not have a lot of current treatments. We are investigating a potential treatment for T-cell leukemia in this study using a new target.
- The Transmethylation (TM) pathway is a vital pathway in leukemic T cells for proliferation and survival.
- The transmethylation (TM) pathway, entails a methyl-transferase-mediated donation of methyl groups by S-adenosylmethionine (SAM) and conversion of SAM to S-adenosylhomocysteine.
- SAH is subsequently hydrolyzed by an enolase enzyme called S-adenosylhomocysteine hydrolase (SAHH) to form adenosine and homocysteine.
- SAH in high amounts acts as a feedback inhibitor of methyltransferases.
- Inhibition of SAHH through pharmacologic inhibitors can induce cell apoptosis using the Fas/Fas ligand pathway, making SAHH a major regulator of the TM pathway and a target for cancer therapy.
- The Fas/FasL pathway is one in which cells undergo apoptosis as a mechanism of death.
- In the current study we investigate the impact of alteration in the SAM:SAH ratio on Fas ligand gene expression and apoptosis.
- We look at the pharmacologic inhibition of SAHH using DZA and DZNeP, and the off target effects that ensues with having high levels of SAH in the cell.
- We examine the formation of the FADD complex over the varying concentrations of DZA, and see if the apoptotic process is occurring.

ACKNOWLEDGEMENTS

Research supported by NCI R25 grant University of Louisville Cancer Center

Education Program NIH/NCI (R25-CA134283

HYPOTHESIS

SAHH Inhibitors increase expression of FasL mRNA and protein and activate the Fas-FasL signaling pathway, inducing cell apoptosis.

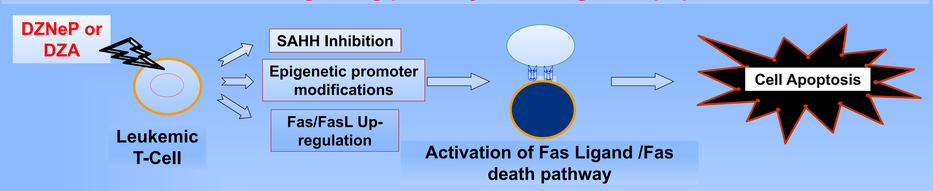

RESEARCH STRATEGY

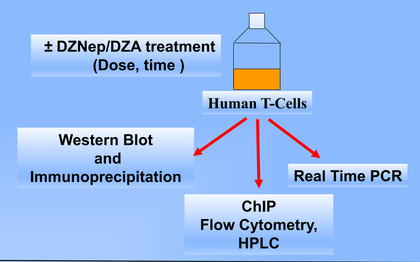

RESULTS

Inhibition of S-adenosylhomocysteine hydrolase (SAHH) Decreases the Cellular Methylation Potential of Human T Leukemic Cells

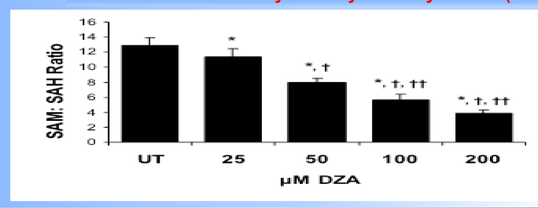

Figure 1: HPLC analysis of cellular S-adenosylmethionine and S-adenosylhomocysteine for Jurkat cells treated with increasing concentrations of DZA for 3 hours.

DZA is well known for its effects as an experimental drug, however an analog to it DZNeP has shown similar properties also has shown favorable effects in clinical trials. DZNeP is currently in clinical phase II

SAHH Inhibition Induces Death Ligand (FasL) Expression in Human T Leukemic Cells

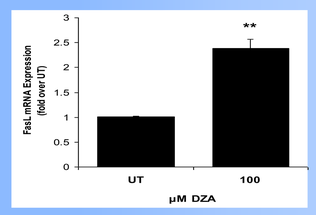

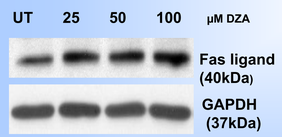

Figure 2: DZA treatment induces FasL mRNA expression in a dose/time dependent manner. These samples were analyzed after cells were treated with 100 uM of DZA for 24 hours.

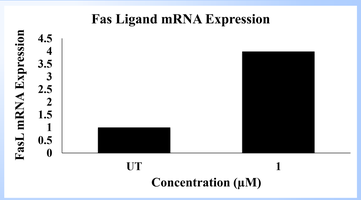

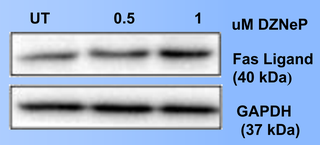

Figure 3: DZNeP treatment induces FasL protein expression. Samples were analyzed after cells were treated with 1 uM of DZNeP for RT-PCR and treated with .5 and 1 uM DZNeP for protein isolates after 12 hours.

SAHH Inhibition and FasL Expression Leads to the formation of the Death Initiating Signaling Complex (DISC) and Apoptotic Signaling in Human T Leukemic Cells

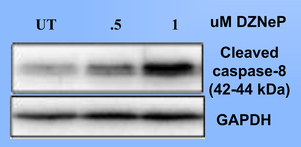

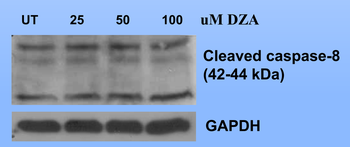

Figure 4: SAHH induces proteolytic activation of caspase-8. Immunoblot analysis was performed using 24 hours lysates for both DZNeP and DZA treated cells.

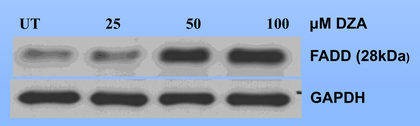

Figure 5: Increase recruitment of FADD with increasing concentrations of DZA treated cells in 24 hours

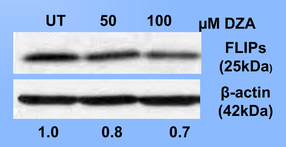

Figure 6: SAHH inhibition decreases FLIPs levels when treated with DZA after 24 hours.

Pharmacologic Inhibition of SAHH Leads to Apoptotic Cell Death in Human T Leukemic Cells

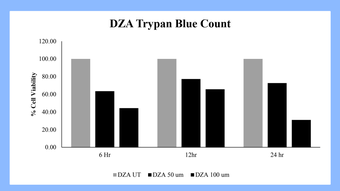

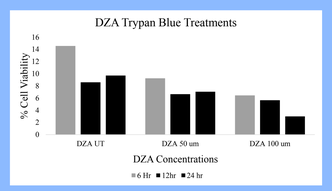

Figure 7: DZNeP/DZA treatment leads to loss of survival of T cell leukemic cells in a dose dependent manner. Jurkat Cells were treated for 24 hours with DZA, and for DZNep Cells were analyzed at 6,12, and 24 hours.

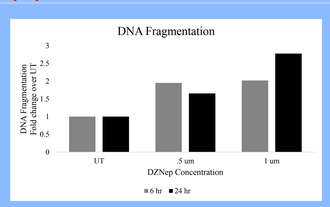

Figure 8: DZNeP induces apoptotic death as indicated by an increase in DNA fragmentation. Cells were treated for 6 and 24 hours

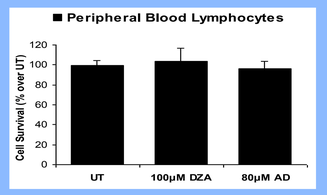

Figure 9: DZA treatment does not affect the survival of primary T lymphocytes. Non-transformed T lymphocytes were subjected to DZA treated and were not affected from the treatment.

MATERIALS AND METHODS

Human Leukemic T Cells: Cultured human leukemic T lymphocytic cells (Jurkat) were propagated in RPMI medium supplemented in 10% fetal bovine serum, 10U/mL penicillin and 10µg/mL streptomycin, and maintained in a 37°C and 5% CO_2 environment. Jurkat cells at a density of $0.25*10^6$/mL were maintained as untreated controls, or treated with DZNeP for 6h (for RNA),12h (for protein), or 24h (for RNA and cell viability).

Cell viability: (A) Trypan Blue Dye Exclusion Assay: Cells were stained with Trypan blue dye, and live and dead cells were counted. **(B) DNA Fragmentation Apoptosis Assay:** The cell death ELISA kit from Roche (Indianapolis IN) was used to detect DNA Fragmentation.

Western Blot analysis: After treatments, cells were lysed with RIPA lysis buffer. The lysates were separated by electrophoresis and detected by immunoblotting.

RNA Isolation and Realtime PCR: Total RNA was isolated using TRIZOL (Invitrogen, Carlsbad, CA). 50 ng of RNA was used for reverse transcription followed by Real time PCR analysis using specific FasL primers and SYBR green I dye on the ABI prism 7500 sequence detection system.

CONCLUSIONS

- Inhibition of SAHH Decreases the Cellular Methylation Potential of Human T Leukemic Cells.
- Inhibition of SAHH leads to upregulation of FasL and formation of Death Inducing Signaling Complex (DISC).
- Inhibition of SAHH induces Fas/FasL mediated apoptosis and decreases cell viability in T leukemic cells.

Overall our data demonstrate that SAHH inhibitors maybe a potential therapeutic strategy for treatment of T cell leukemia

FUTURE DIRECTIONS

- Investigate Detailed Mechanisms underlying SAHH inhibition-induced T leukemic cell apoptosis.
  - Epigenetic transcriptional regulation of FasL gene.
  - Analysis of DISC formation with DZNeP.
  - Examine the effect DZNeP has on primary non-transformed lymphocytes.
- Validate our findings in T-cells from patients who have T-cell leukemia.
- Conduct pre-clinical studies of DZNeP in T cell leukemia patients.

Biomarker Significance of Exosomes During Breast Cancer Initiation and Progression

Kendall Huddleston[a], Farrukh Aqil[bc], Ramesh Gupta[a,b,] and Radha Munagala[b,c]

[a]Department of Pharmacology and Toxicology, [b]James Graham Brown Cancer Center,
Department of Medicine[c], University of Louisville

Introduction

- The American Cancer Society estimates approximately 232,670 new cases of invasive breast cancer in women in the United States for 2014, with an estimated 40,000 deaths[1].
- Women who have prolonged elevated estrogen levels have a higher susceptibility to be diagnosed with breast cancer.
- Current methods of breast cancer diagnosis require invasive methods such as a biopsy.
- Exosomes are endosomal vesicles (~40-200 nm) that are released from all cell types and can be found in most or all bodily fluids[2].
- Recent studies show that exosomes are released more abundantly from tumor cells than normal cells[3].
- Exosomes facilitate intercellular communication via the unique cargo it carries including lipids, proteins, RNA and miRNAs[2].
- We hypothesize that exosomes could be used as a potential biomarker for the initiation and progression of breast cancer.

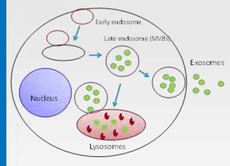

Fig 1a. Exosome biogenesis occurs during the inward membrane budding of the multivesicular body. These MVBs then release the exosomes through fusion of the cell membrane.[3]

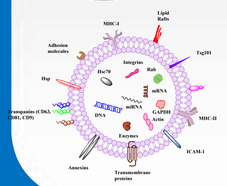

Fig 1b. Inner cargo and surface proteins located on exosomes. Main proteins looked at during this study: Alix, CD63, CD81, CD44, and β-actin.

Results

Exosome Size Determination

Table 1. Exosome size (nm) and polydispersion index (PDI) of serum exosomes.

	C10	133.0	0.34
7 m Control	A8	129.6	0.40
	A14	153.8	0.40
7 m E2	C15	104.8	0.38
	C30	51.9	0.65

Protein Yield of Serum-Exosomes

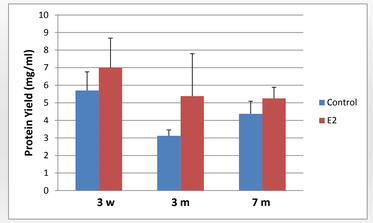

Fig 2. Mean protein yield (mg/ml) of serum-derived exosomes at different time points (n=4). Statistical analysis was done using paired t-test.

Protein Yield of CD63-Enriched Exosomes

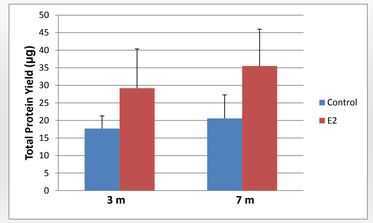

Fig 3. Total protein yield (µg) of CD63-enriched exosomes. Two hundred µg of exosomes isolated by precipitation method were used for enrichment with CD63 magnetic beads (n=3). Statistical analysis was done using paired t-test.

Alix

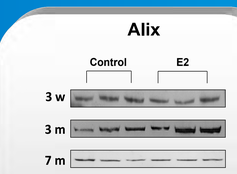

Fig 4a. Western blot analysis depicting the expression levels of Alix from 3 w, 3 m, and 7 m control and E2-treated serum exosome samples.

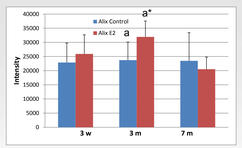

Fig 4b. Mean intensity quantification of Fig. 4a using ImageJ software. Statistical analysis was done using paired t-test. (p value=0.028) β-actin served as loading control. (n=3).

CD44

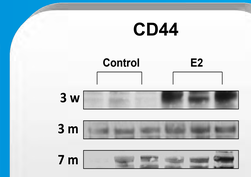

Fig 5a. Western blot analysis depicting the expression levels of CD44 from 3 w, 3 m, and 7 m control and E2-treated serum exosome samples.

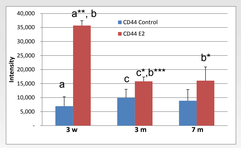

Fig 5b. Mean intensity quantification of Fig. 5a using ImageJ software. Statistical analysis was done using paired t-test. a**:p value=0.0018; b*:p value= 0.0187, b***: p value= 0.00002 and c*: p value=0.032. β-actin served as loading control.(n=3).

CD63

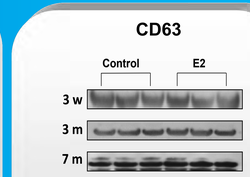

Fig 6a. Western blot analysis depicting the expression levels of CD63 from 3 w, 3 m, and 7 m control and E2-treated serum exosome samples.

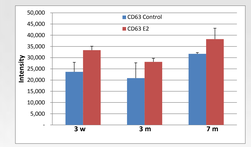

Fig 6b. Mean intensity quantification of Fig. 6a using ImageJ software. Statistical analysis was done using paired t-test. β-actin served as loading control.(n=3).

CD81

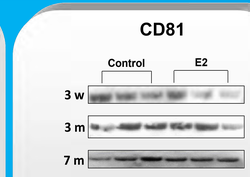

Fig 7a. Western blot analysis depicting the expression levels of CD81 from 3 w, 3 m, and 7 m control and E2-treated serum exosome samples.

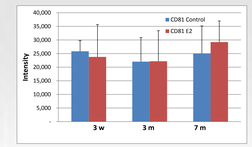

Fig 7b. Mean intensity quantification of Fig. 7a using ImageJ software. Statistical analysis was done using paired t-test. β-actin served as loading control.(n=3).

EGFR

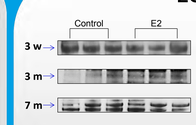

Fig 8a. Western blot analysis depicting the expression levels of EGFR from 3 w, 3 m, and 7 m control and E2-treated serum exosomes

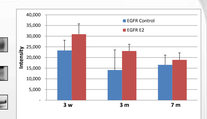

Fig 8b. Mean intensity quantification of Fig. 8a using ImageJ software. Statistical analysis was done using paired t-test. β-actin served as loading control.(n=3).

EGFR on CD63-Enriched Exosomes

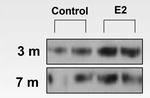

Fig 9a. Western blot analysis depicting the expression levels of EGFR from 3 w, 3 m, and 7 m control and E2-treated CD63 enriched serum exosomes

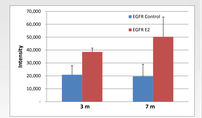

Fig 9b. Mean intensity quantification of Fig. 9a using ImageJ software. Statistical analysis was done using paired t-test. β-actin served as loading control.(n=3).

Key Findings

- Exosomes isolated from serum samples were in the size range of 40-200 nm.
- The mean exosomal protein yields of E2-treated samples were higher than their respective control for each time period. However, the differences did not attain statistical significance.
- Enrichment of serum exosome using CD63 magnetic beads resulted in higher protein yield in a) E2-treated than control and b) 7 m E2-treated compared to 3 m E2-treated samples; however, these differences did not attain statistical significance.
- Serum derived-exosomes were positive for hallmark exosomal proteins, including Alix, CD81, CD63 and CD44.
- Expression levels of Alix and CD44 were significantly higher in E2-treated serum exosomes compared to control. While this trend was also observed with other exosomal markers, this difference did not attain statistical significance.
- Previous reports indicate CD44 positive exosomes to have the ability to increase extracellular matrix degradation and augment tumor invasion[4].
- Estrogen growth factor receptor (EGFR) expression levels were higher in E2-treated serum exosomes compared to control; this difference was even greater after enrichment for CD63-positive exosomes.
- Our preliminary observations suggests the potential of serum exosomes to reflect the increase in proliferation of rat mammary tissue. However, significance was not attained for either condition presumably due to small samples size.

Conclusions

Higher levels of serum exosomes positive for exosomal surface proteins and proliferation markers with E2-treatment indicate their potential as biomarker during initiation and progression of breast cancer.

Future Directions

- **Increase sample size to reduce deviations**
- **Use enrichment techniques to improve quality of data**
- **Correlate data to tumor size and multiplicity for each animal**

Methods

- **ACI Rat Model**: Female ACI rats (5-6 week old) were acclimatized for 1 week on rat chow diet and later fed either purified AIN-93M diet. Two weeks later, animals were implanted with 1.2-cm long silastic implant containing 9 mg of 17β-estradiol. Body weight, diet consumption and tumor incidence were monitored weekly until euthanasia. Animals with euthanized after 3 weeks (3 w), 3 months (3 m) and 7 month (7 m). Serum was separated from blood for further analysis.

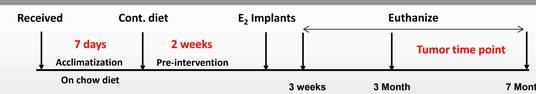

- **Exosome Isolation**: Total Exosome Isolation (from serum) reagent (Invitrogen, Carlsbad, CA) was added to each serum sample (100 µl). After incubation at 4°C for 30 min, the sample was centrifuged at 10,000 x g for 10 min at room temperature. Exosomes were suspended in 50-100 µl of PBS.
- **Exosome Enrichment**: Isolated exosomes were enriched using CD3-captured magnetic beads. Beads were washed 3 times with 0.1% BSA in PBS and exosomes sample was incubated overnight at 4°C with continuous mixing. At the end of incubation the beads were washed 3 times and, CD63-specific exosomes were eluted using RIPA lysis buffer.
- **Exosome Size Determination**: Zetasizer Nano (Malvern, Westborough, MA) was used to determine the average size and polydispersion index (PDI) of exosomes isolated from serum. Samples of 50 µl were appropriately diluted and analyzed by measuring the dynamic light scattering.
- **BCA Protein Assay**: The protein concentration was determined by using a BCA Protein Assay Kit (Pierce, Rockford, IL), where the serum exosomes were ran against known standards. After 30 minute incubation in 37°C, optical density was measured at 562 nm using UV-visible spectrophotometer (Molecular Devices,Sunnyvale, CA).
- **Western Blot Analysis**: 30 µg protein was loaded and separated on SDS PAGE gel and then transferred to PVDF membrane. Each membrane was blocked using either 4% non-fat dry milk or 4% BSA, and the appropriate primary antibody was added (Alix, EGFR, CD81, CD63, and CD44) overnight at 4°C. After washing, membranes were probed with HRP-conjugated secondary antibody. Proteins were analyzed using chemiluminescent kits. Blot intensities were quantified using imageJ software. Statistical analysis was determined using Sigma Plot software.

References

1. American Cancer Society. Cancer Facts & Figures 2014. Atlanta: American Cancer Society; 2014.
2. Vlassov, Alexander (2012). Exosomes: Current knowledge of their composition, biological functions, and diagnostic and therapeutic potentials. Biochimica et Biophysica Acta, 2012. 1820: 940-980
3. Ludwig, Anna-Kristin Exosomes: Small vesicles participating in intercellular communication. International Journal of Biochemistry and Cell Biology, 2011. 44: 11-15
4. Yang, Chenjie and Robbins, Paul. The Roles of Tumor Derived Exosomes in Cancer Pathogenesis. Clin Dev Immunol. v2011; 2011: 842849.

Research supported by University of Louisville Cancer Education Program and NCI grant R25-CA 1344238, Agnes Brown Duggan Endowment and Hemsley Funds.

The Role of Carbon Chain and Carbonyl Group in AHL-induced Caspase-9-dependent Apoptosis

Jaison John, B.A., Nicole S. Stivers, M.S., Aaron M. Neely, M.S., Guoping Zhao, Ph.D., John Eaton, Ph.D., Chi Li, Ph.D.
Department of Pharmacology and Toxicology, Brown Cancer Center, University of Louisville School of Medicine

UNIVERSITY OF LOUISVILLE

Abstract

N-Acyl-Homoserine lactones (AHLs) are essential quorum-sensing molecules that play vital roles, such as regulating virulence factors in pathogens. Our interest has been sparked by C12, an AHL produced by the opportunistic bacterium, *Pseudomonas aeruginosa*. We have recently discovered that C12 induces human tumor cell apoptosis, following a pathway that is caspase-9-dependent. Recent studies have also found that it preferentially kills transformed cells over normal cells. For this study, our goal was to identify other AHLs that induce caspase-9-dependent apoptosis. WT and Caspase-9 KO Mouse Embryonic Fibroblast (MEF) cells were treated with increasing concentrations of various derivatives of C12 for 24 hours. We found that reduction of the carbon chain length by treating with C6 and C8, eliminated the ability to induce cell death based upon the propidium iodide (PI) assay. However, C14, with increased carbon chain length, like C12 was able to induce the apoptosis cascade. Simply removing the carbonyl group from C14, forming C14 HSL, resulted in a completely different cell death pathway independent of caspase-9. We suspect that pathway to be autophagy, as many of the cells have an accumulation of LC3-B positive autophagosomes and are not Annexin V or PI positive. Our results indicated that both the carbon chain length and carbonyl group are important for AHL-induced caspase-9-dependent apoptosis.

Results

1 C12 and C14 induce apoptotic cell death in MEF cells

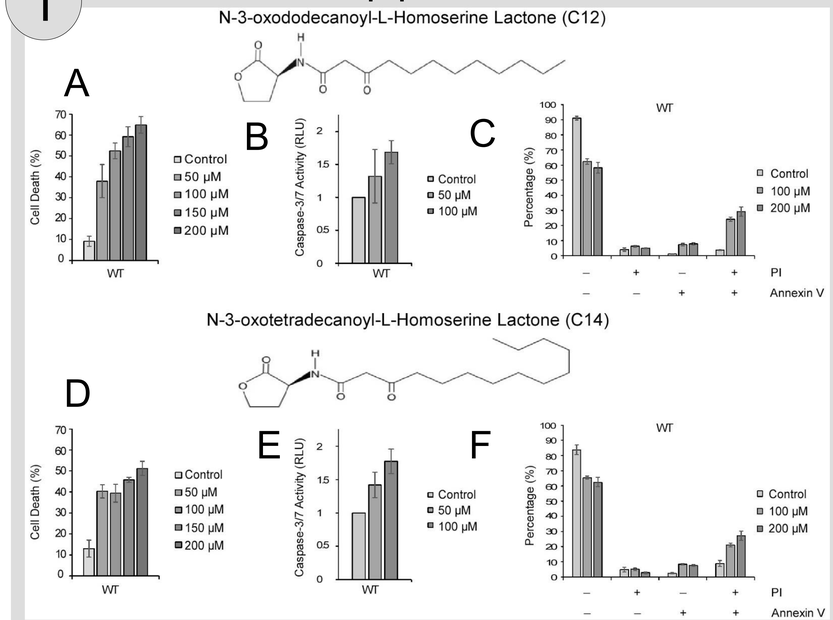

Figure 1: (A-C) Upon 24 hours-treatment with various concentrations of C12 in MEF WT cells, the percentage of PI positive cells (A), relative caspase-3/7 activity (B), and annexin V positive cells (C) were measured. (D-F) MEF WT cells were treated with C14 for 24 hours and the percentage of PI positive cells (D), relative caspase-3/7 activity (E), and annexin V positive cells (F) were measured.

Results

2 The Cytotoxicity of AHLs is dependent on the length of the carbon tail

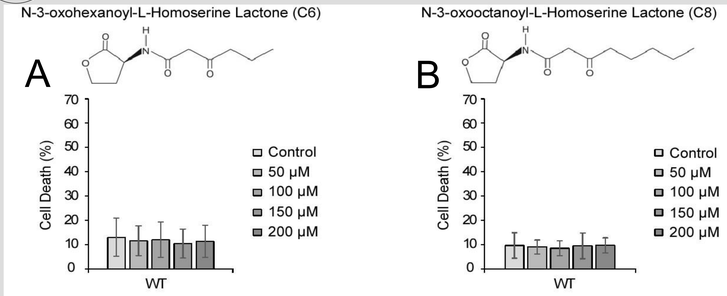

Figure 2: (A-B) C6 and C8, which have shorter carbon chain length, have no cytotoxic effects on the WT MEF cells after 24 hours-treatment.

3 The carbonyl group is essential for both C12 and C14 induced apoptosis

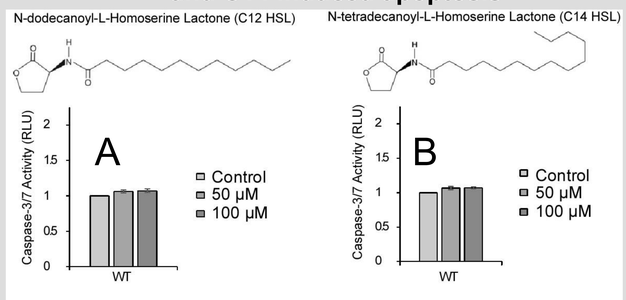

Figure 3: (A-B) No apoptosis was found in MEF cells following 24 hour-treatment with C12 HSL and C14 HSL, which have no carbonyl group.

4 C12 and C14 induce caspase-9-dependent apoptosis.

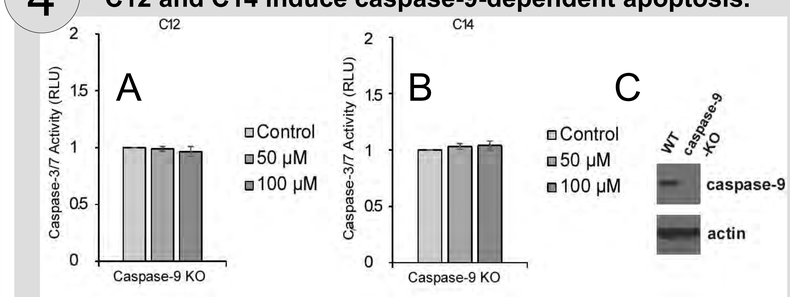

Figure 4: (A-B) Caspase-9 KO MEF cells were treated with increasing concentrations of C12 (A) and C14 (B) for 24 hours. There was no caspase-3/7 activity relative to control. This suggests that the induction of apoptosis by C12 and C14 is dependent upon caspase-9. (C) Western blot showing caspase-9 expression in MEF cells.

5 C14 HSL induces caspase-9-independent cell death through autophagy

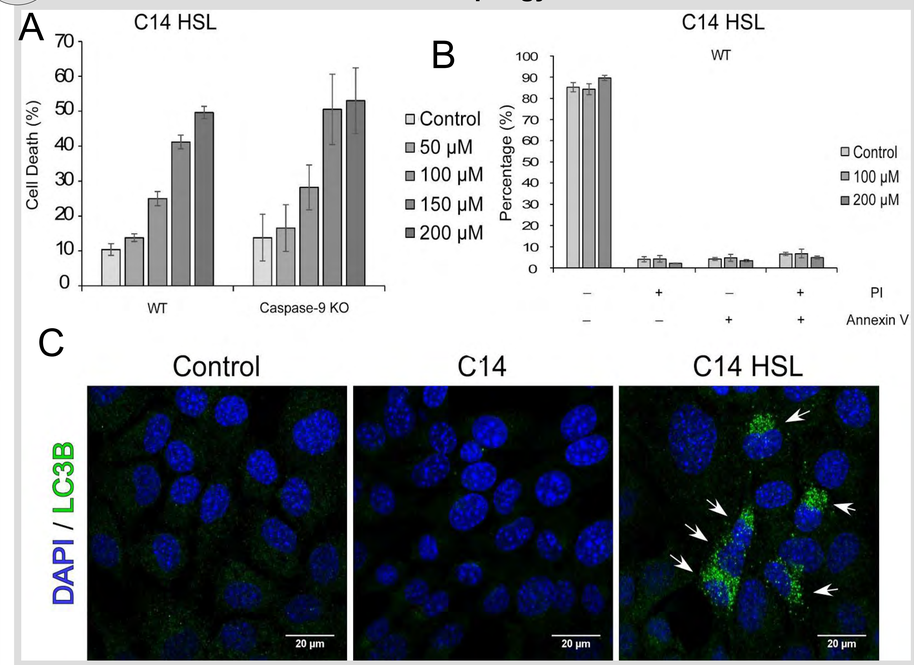

Figure 5: (A) WT and Caspase-9 KO MEF cells were treated for 24 hours with increasing concentrations of C14 HSL. Both WT and Caspase-9 KO cells were killed by C14 HSL. (B) Percent annexin V positive cells was measured in WT MEF cells following 24 hours-treatment with C14 HSL. (C) 60X Maximum Intensity Projection confocal images are shown of MEF WT cells treated for 24 hours with either vehicle control, 200µM C14, or 200µM C14 HSL. Arrows point to LC3-B markings.

Conclusions

- C12 and C14 induce caspase-9-dependent apoptotic cell death in MEF cells.
- Reducing the length of carbon chain decreases the cytotoxicity of the AHLs, C12 and C14.
- The carbonyl group is vital for both C12 and C14 induced apoptosis.
- C14 HSL, which lacks the carbonyl group, causes cell death through autophagy but not through apoptosis or necrosis.

Acknowledgements

- Research was supported by a grant from NCI R25 grant University of Louisville Cancer Education Program NIH/NCI (R25-CA134283) and the School of Medicine Summer Research Scholar Program.

Cannabigerol Modulates the Efficacy of Cannabinoids On CB2 Receptor

Alyssa S. Laun, Pritesh P. Kumar, Zhao-Hui Song
Department of Pharmacology and Toxicology
University of Louisville School of Medicine

Abstract

Cannabigerol (CBG) is a non-psychoactive phytocannabinoid. It is currently unknown what the interaction of CBG is with the cannabinoid receptor 2 (CB2). This project measured the modulation of CBG on the effects of known cannabinoid agonists including endo- and synthetic cannabinoids. A homogeneous time resolved fluorescence method was used to quantify CB2 mediated decrease in cyclic adenosine monophosphate (cAMP) levels. CBG by itself had no effect on cAMP levels. However, CBG was found to increase the efficacy of AEA and WIN55,212-2, but no effect was observed on the other cannabinoids.

Introduction

CBG was first identified by Gaoni an Mechoulam in 1964. This phytocannabinoid has multiple potential targets including Cox1/2 enzymes, TRP channels, cannabinoid, 5-HT, α_2 adrenergic, and $PPAR_\gamma$ receptors. CBG has been shown to exhibit antiproliferative and pro-apoptotic on a number of human cancer cell lines. CB2 is a G protein coupled receptor found primarily in the peripheral tissues of the immune system, but not extensively in the CNS. CB2 ligands have immunomodulary, anti-inflammatory, and pain modulatory effects.

Methods

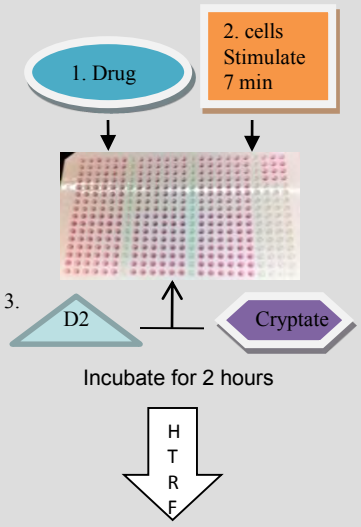

4. 337 nm light to excite cryptate transfer from cryptate to D2- labeled cAMP

5. 2 wavelengths, 665 and 620 nm to measure emission

Results

A

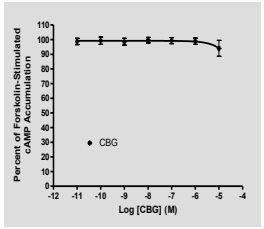

B

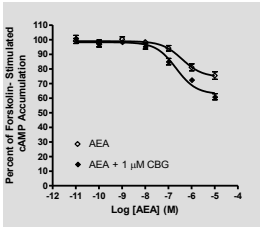

C

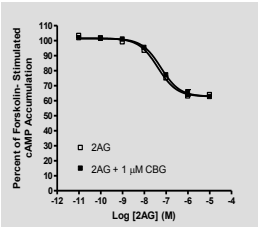

Figure 2A. Effect of CBG on Forskolin- stimulated cAMP accumulation. HEK293 cells stably expressing CB2 were treated with different concentrations of CBG.

Figure 2B,C. Modulation of endocannabinoid- induced inhibition of forskolin-stimulated cAMP accumulation by CBG. HEK 293 cells stably expressing CB2 were pre-incubated for 10 minutes with vehicle or 1 μM CBG before subject to stimulation with (B) AEA or (C) 2AG for 7 minutes. Results are expressed as percent forskolin- stimulated cAMP accumulation.

D

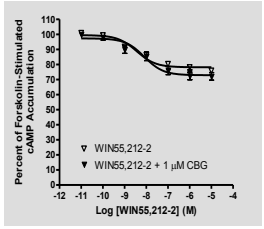

E

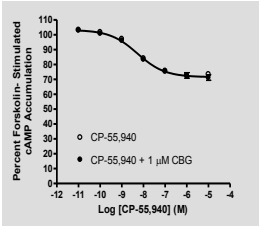

F

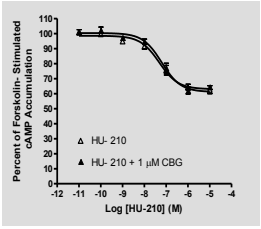

Figure 2D,E,F. Effect of CBG on forskolin- stimulated cAMP accumulation by synthetic cannabinoids. Cells stably expressing CB2 were pre-incubated with vehicle or 1 μM CBG for 10 minutes before subject to stimulation with synthetic cannabinoid agonists (D) WIN55,212-2, (E) CP-55,940, and (F) HU-210 for 7 minutes. Results are expressed as percent forskolin- stimulated cAMP accumulation.

Figure 1: Structures of Cannabinoids used

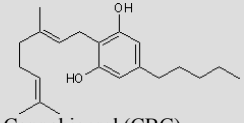

Cannabigerol (CBG)

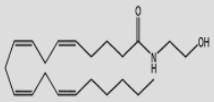

N-arachidonoylethanolamine (AEA)

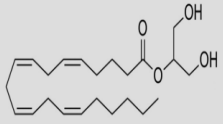

2-Arachidonoylglycerol (2AG)

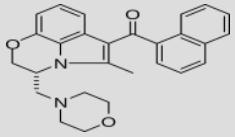

WIN55,212-2

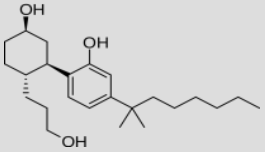

CP-55,940

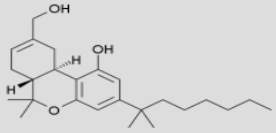

HU-210

Conclusions

1. CBG alone did not affect forskolin- stimulated cAMP accumulation at concentrations up to 10 μM.
2. CBG did not modify cAMP inhibition induced by synthetic cannabinoids CP-55,940 or HU-210, or endocannabinoid 2AG.
3. CBG increased the efficacy of cAMP inhibition induced by endocannabinoid AEA and synthetic WIN55,212-2.

Acknowledgements

This research was partially supported by NCI grant R25 CA134283 to the University of Louisville

The Novel Interaction of NORE1A and RIT in Lung Cancer

Michael A. Mannen[1], M. Lee Schmidt[2], and Geoffrey J. Clark[3]

Departments of Biology[1], Chemistry[1], Biochemistry & Molecular Biology[2], and Pharmacology & Toxicology[3]

School of Medicine, University of Louisville

INTRODUCTION

Lung cancer remains the largest cause of cancer related deaths and diagnosis worldwide [1]. Lung cancer cases are classified based on size and biochemical alterations in the cells of origin, with non-small cell lung carcinomas being the predominant form witnessed clinically [2]. Mutations in the Ras gene remain a signature genetic contributor to development of non-small cell lung carcinomas and can be found in roughly 30% of cases [3, 4].

Members of the RAS Subfamily, class of small GTP-ase proteins, have long been implicated in the etiology of lung cancers and play an important role in cell signal transduction [5]. Activated RAS contributes to a pro-growth and survival phenotype mediating the hallmarks of cancer by activating and suppressing an array of effectors with many downstream targets associated with diverse changes in cell behaviors [5]. NORE1A (RASSF5) is a novel RAS death effector and potent tumor suppressor [6]. It functions by interacting with other apoptotic effectors thereby promoting the pro-apoptotic effects of RAS [6]. Death effectors of RAS are believed to serve as a protection mechanism against over-stimulation of RAS signaling, and loss of these negative effectors of RAS shifts the cell toward transformation [6]. NORE1A is suppressed by an epigenetic mechanism in at least 30% of NSCLC. Recently, a novel branch of the RAS Superfamily has also recently been identified as having a role in the establishment and progression of lung cancer [7]. Activating mutations have now been detected in the RIT protein in lung cancer [7]. RIT (Ras-like protein in tissues) is remarkably similar to RAS in both domain and sequence homology and it has been shown to powerfully induce activation of p38, ERK, and AKT signaling depending on cellular context [7].

The mechanisms with which Rit drives cellular transformation remain only partially characterized. A yeast-two hybrid screen identified wild type RIT as a binding partner of NORE1A. We sought to determine if this interaction could be detected in mammalian cells and if there are any functional consequences of the interaction for lung cancer cells. Here we show that RIT does in fact complex with NORE1A in cells and acts to suppress the pro-apoptotic and tumor suppressor phenotype of NORE1A.

METHODS

Cell Lines: HEK293, HEK293T, and NCI-H1299 cells were maintained in DMEM supplemented with 10% fetal bovine serum (FBS) and 1% penicillin-streptomycin and RPMI supplemented with 10% FBS and 1% penicillin-streptomycin, respectively.

Luciferase Assay: PUMA signaling was measured by luciferase assays using the PUMA-Luc promoter construct with the Promega Dual Luciferase System.

Protein Analysis: Protein expression was monitored by transfection of HEK293, HEK293T or NCI-H1299 cells and Western blotting analysis. Immunoprecipitations were performed with GFP-conjugated sepharose beads.

RESULTS

1

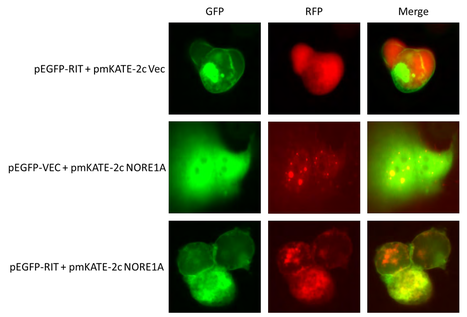

HEK293 cells were transfected with expression constructs expressing GFP (pEGFP-C1), RFP (pmKate-2C), pEGFP-RIT, and pmKate-NORE1A. The cells were photographed 24 hours post-transfection under UV stimulation. RIT and NORE1A show a high degree of localization proximal to the plasma membrane.

2

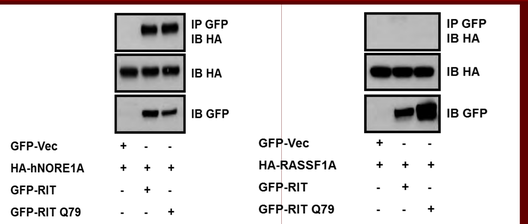

HEK293T cells were transfected with expression constructs for HA-NORE1A, HA-RASSF1A (closely related RASSF family member), GFP-RIT, and a constitutively active RIT (GFP-RIT Q79). Cells were lysed 24 hours post-transfection and immunoprecipitated with GFP-agarose beads, and analyzed on a Western blot. Results show that NORE1A binds to RIT independently of its activation status. Interestingly, this interaction with RIT does not seem to be shared across the RASS family, making this a novel and specific interaction with NORE1A.

3

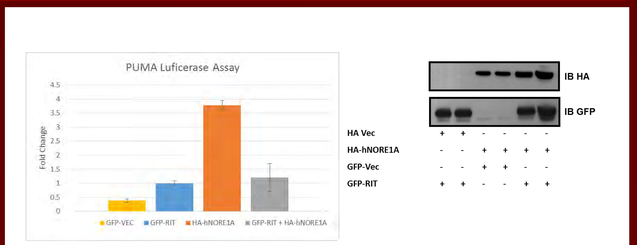

HEK293 cells were transfected with expression constructs for HA-NORE1A, GFP-RIT, Vector (Control), and PUMA-LUC Reporter construct. 24 hours post-transfection, cells were lysed with a reporter lysis buffer, and assayed with a Luciferase Reporter Kit (Promega). Relative Light Units were converted to Fold Change for analysis. The lysates were also run on a Western blot to determine relative levels of protein expression.

4

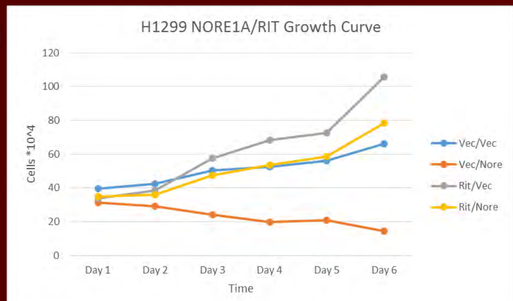

NCI-H1299 (deficient for NORE1A expression) Cells were transfected and stabilized with either pZip-HA-VEC or pZIP-HA-NORE1A resulting in a +/- NORE1A system. This system was subsequently transfected with expression constructs for GFP-RIT or empty vector. Equal number of cells of each line were plated. Cells were then trypsinized and counted daily for a period of 6 days. This experiment suggests that RIT overrides NORE1A's growth suppression in NCI-H1299 Cell line.

5

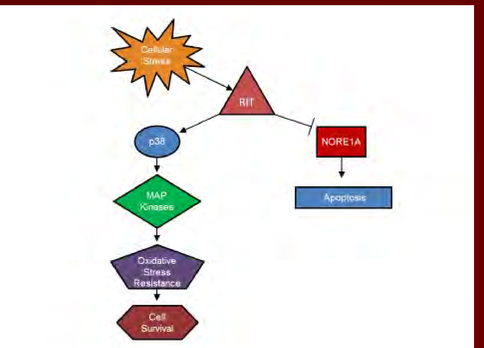

Proposed signaling pathway where RIT suppresses NORE1A's ability to activate apoptotic signaling. Our data suggests that RIT drives transformation by subduing NORE1A mediated tumor suppressive functions, however, the mechanisms involved here remain largely undefined. Future experiments are necessary to further characterize the consequences of the RIT/NORE1A interaction on cellular transformation.

CONCLUSIONS

Only recently has RIT surfaced as a protein of interest in the etiology of lung cancer. Better understanding of the molecular mechanisms involved are integral in the pursuit of successful drug development. Our research now shows that RIT and NORE1A bind and suggests that this interaction has an effect on cellular growth and survival. Our data advocates that RIT works to suppress NORE1A mediated pro-apoptotic pathway signaling, resulting in increased growth and survival non-small lung carcinoma growth in vitro.

ACKNOWLEDGEMENTS

This work was supported by NCI R25-CA134283 Cancer Education Grant awarded to the University of Louisville and R01 CA133171-01A2 funded to GJC. Additionally, would like to thank Dr. Clark for his mentorship, Lee Schmidt for his training and mentorship, and the entire Clark Lab Staff for their entertainment and patience.

REFERENCES

1. United States Cancer Statistics. 2013; Available from: http://www.cdc.gov/cancer/lung/statistics/.
2. General Inforamtion About Non-Small Cell Lung Cancer. 2014; Available from: http://www.cancer.gov/cancertopics/pdq/treatment/non-small-cell-lung/Patient/page1.
3. Imielinski, M., et al., Mapping the hallmarks of lung adenocarcinoma with massively parallel sequencing. Cell, 2012. 150(6): p. 1107-20.
4. Seo, J.S., et al., The transcriptional landscape and mutational profile of lung adenocarcinoma. Genome Res, 2012. 22(11): p. 2109-19.
5. Riely, G.J., J. Marks, and W. Pao, KRAS mutations in non-small cell lung cancer. Proc Am Thorac Soc, 2009. 6(2): p. 201-5.
6. Clark, G.J., et al., RASSF Family Proteins. Mol Biol Int, 2012. 2012: p. 938916.
7. Berger, A.H., et al., Oncogenic RIT1 mutations in l

Breast Cancer Diagnosed through the Mobile Mammography Van in Jefferson County, KY

S Mudra[1], J Pan[2] , SN Rai[2], EC Riley[1]

Department of Medicine, Division of Oncology/Hematology[1] and Department of Bioinformatics and Biostatistics[2]

James Graham Brown Cancer Center, University of Louisville School of Medicine

BACKGROUND

- The purpose of this study is to investigate and understand demographic, clinical and biologic trends among breast cancer patients diagnosed through the Mobile Mammography Unit (MMU) in Jefferson County, KY from 2000-2010.
- This study is a retrospective institutional review designed to examine demographic, clinical and biologic trends among women diagnosed with invasive breast cancer or DCIS via the MMU.

MATERIALS AND METHODS

- 21,857 individuals visited the MMU during the study period.
- 247 unique subjects were identified through the database as requiring biopsies.
- 165 individuals were ineligible for analysis due to benign pathology or high risk status.
- Data were unavailable for 4 patients because surgical consult was recommended; however, pathology was unavailable for review (e.g. went to another institution).
- 78 invasive cancers (stage I, II, III) or DCIS treated at our institution remained for analysis.
- Demographic data (age, race and insurance status) and clinical and biologic factors (histologic diagnosis, biologic subtype, stage, BMI and family history) were collected on those with a cancer diagnosis.
- For categorical variables, the descriptive statistics frequency, percentage and cumulative percentage, related to different predictors (such as race, age and insurance) were produced using SAS procedure FREQ. All calculations were performed with SAS statistical software (SAS, 2003).

ACKNOWLEDGEMENTS

- University of Louisville Cancer Education Program NIH/NCI (R25-CA134283)

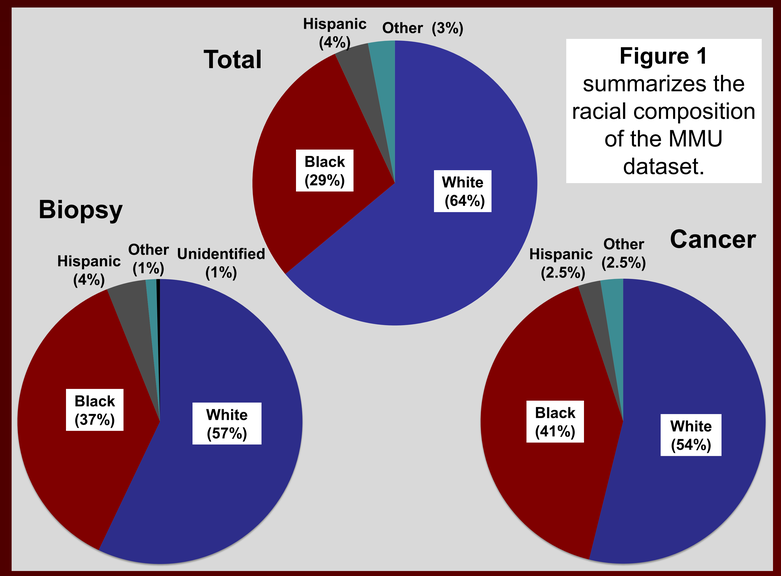

Figure 1 summarizes the racial composition of the MMU dataset.

Table 1: Insurance	Total (N=21, 857)	Biopsy (N=247)	Cancer (N=78)
Insured	12, 435 (57%)	56 (23%)	29 (37%)
Uninsured	9, 422 (43%)	191 (77%)	49 (63%)

Table 2: Clinical and Biologic Factors

Variable	Cancer (N=78)
Histologic Diagnosis	
IDC	55 (71%)
DCIS	18 (23%)
ILC	3 (4%)
IDC/ILC	1 (1%)
Other	1 (1%)
Stage	
0	17 (22%)
I	19 (24%)
II	11 (14%)
III	4 (5%)
Unavailable	27 (35%)

Variable	Cancer (N=78)
ER/PR	
Positive	58 (74%)
Negative	15 (19%)
Unavailable	5 (6%)
Triple Neg	
No	60 (77%)
Yes	6 (8%)
Unavailable	12 (15%)
Her2Neu	
Positive	10 (13%)
Negative	48 (61%)
Unavailable	20 (26%)

Variable	Cancer (N=78)
Age	
40-49	20 (26%)
50-59	26 (33%)
60-69	23 (29%)
70+	9 (12%)
BMI	
Underweight	1 (1%)
Normal	8 (10%)
Overweight	12 (16%)
Obese	26 (33%)
Unavailable	31 (40%)
Family History	
Yes	19 (24%)
No	24 (31%)
Unavailable	35 (45%)

RESULTS

- Most women diagnosed with cancer were uninsured (63%), despite a majority of insured women (57%) visiting the MMU (Table 1).
- Consistent with the known incidence of biologic subtypes of breast cancer, DCIS was 23% of diagnoses (Table 3).
- Consistent with the goals of mammography, early stage breast cancer (stage 0, I, or II) represented nearly half of the diagnoses. Locally advanced disease (stage III) only represented 5%, although 35% of staging data are unavailable for review.
- Cancers diagnosed were more likely to be ER positive. Triple negatives represented only 8% of diagnoses. 13% of tumors were Her2Neu positive.
- Over ¼ of the cancer dataset was individuals aged 40-49.

CONCLUSIONS

- A higher density of breast cancer was observed among black women, with blacks representing 41% of all cancer diagnoses.
- Additionally, over ¼ of women diagnosed were aged 40-49, a higher incidence than would be expected given historical controls.
- Although there was a higher cancer incidence among black and uninsured women, these data may be biased given this is the targeted population of the MMU.
- Known risk factors for breast cancer, namely obesity and family history, were consistent with the dataset.
- Due to the retrospective nature of this study, large amounts of data were unavailable for review. Therefore, results should be confirmed with additional studies.
- Despite these limitations, this dataset suggests that cancer incidence among historically disadvantaged populations (blacks, uninsured) as well as younger aged women may be disproportionately high in Jefferson County and should be analyzed in a larger study to confirm this finding.

Identification of an Internal Reference microRNA from the Plasma of Multiple Cancer Types

Alexander Myers, Henry Roberts BS, Jonathan Rice MD, Robert Eichenberger MS, Susan Galandiuk MD

Hiram C. Polk Jr. MD Department of Surgery, University of Louisville School of Medicine, Price Institute of Surgical Research and the Section of Colorectal Surgery, Louisville, KY

Introduction

MicroRNAs are commonly investigated as diagnostic and prognostic markers in tissue and biofluids in various diseases. They have been found to be very sensitive and specific biomarkers for many diseases

Absolute quantification uses a known quantity, of a synthetic microRNA, to establish a standard curve

It Allows the researcher to determine the exact number of microRNA copies, prior to amplification, for a given polymerase chain reaction (PCR) signal

Relative quantification uses an endogenous housekeeping microRNA to compare or standardize with their microRNA of interest

- Although U6 and miR-16 is regularly used, there is much debate about the selection of optimal endogenous control(s) in plasma
- We chose this method because it attempts to establish a control for the known genetic variability between individuals

Characteristics of an optimal reference microRNA

- Expresses in all samples
  - Cannot analyze any data if reference microRNA did not express
- Consistent Expression
  - Similar Cycle threshold value regardless of the experimental group or condition

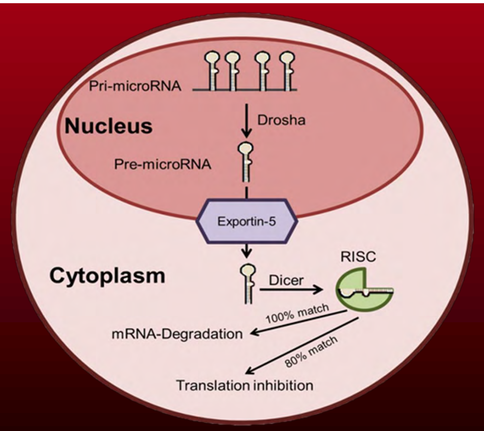

Billeter et al., Seminars Thoracic Cardiovascular Surgery, 2012

Methods and Materials

Our study investigated endogenous reference microRNA expression in plasma from a variety of different neoplasias

- **Colorectal Cancer (n=20)**
- **Colorectal Adenoma (n=10)**
- **Breast Cancer (n=10)**
- **Lung Cancer (n=10)**
- **Pancreatic Cancer (n=10)**
- **Controls (n=10)**

Peripheral blood was collected from all patients and plasma was isolated

Total RNA was extracted using Ambion TRIzol LS Reagent Protocol and measured with a Nanodrop 2000 Spectrophotometer.

cDNA was produced for 381 microRNAs by reverse transcription, with Megaplex Reverse Transcription Pool A v2.1 (Life Technologies, Foster City, CA)

After preamplification, quantitative Real-Time Polymerase Reaction (PCR) was preformed using a 381 microRNA TaqMan low-density array card (TLDA) with a ViiA™7 Real-Time PCR system (Life Technologies, Foster City, CA)

A fixed cycle threshold bar of 0.03 was for all screening arrays

The mean and standard deviation were calculated for each microRNA in each group

microRNAs were assessed for minimal standard deviation in each group and then analyzed for consistent means across the groups

Review Results

We conducted a literature review of 203 publications on the subject of “plasma microRNAs” from the first half of 2014. We queried three main questions

- Did the publication use absolute or relative quantification?
- If it used relative quantification, than which reference microRNA(s) was used?
- If it used absolute quantification, which spike in control was used?

- Relative quantification was used 69% of the time, whereas 31% used absolute quantification
- For absolute quantification, 88% of the absolute papers used cel-miR-39
- For relative quantification, miR-16 (30%) and U6 (25%) were the two most commonly used housekeeping microRNAs, between the relative papers

Reference MicroRNA Analysis Results

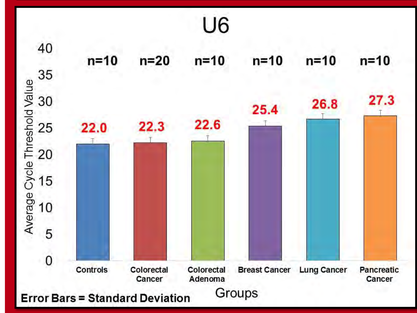

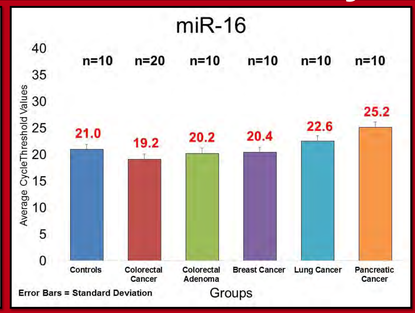

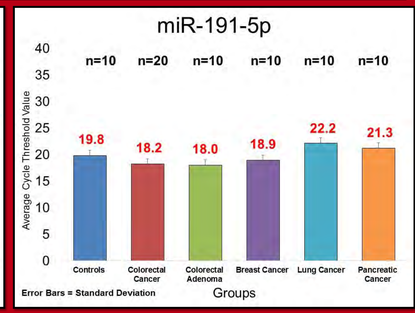

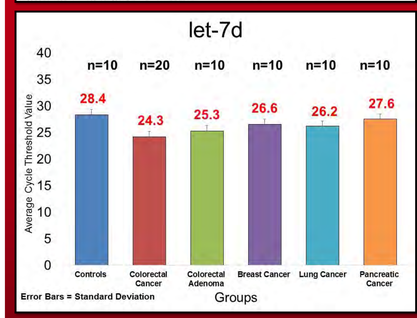

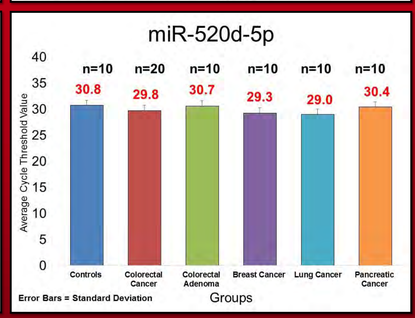

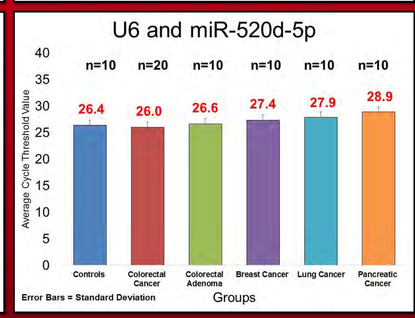

Conclusions

In the current plasma microRNA literature, relative quantification method is used much more frequently as compared absolute quantification. Thus selection of an optimal reference microRNA is critical for reproducible and potentially clinically relevant plasma microRNA results. Overall, we concluded that a combination of U6 and miR-520d-5p provides the greatest stability within each group examined and across the different groups.

Acknowledgements

National Cancer Institute grant R25-CA134283, John W. and Caroline Price Family Trust as well as Donald and Irene Dizney